Partial-Wave Analysis of the $\eta\pi^+\pi^-$ System Produced in the Reaction $\pi^- p \to \eta\pi^+\pi^- n$ at 18 GeV/c

Version 0.1

E852 Collaboration

J. J. Manak, T. Adams, J. M. Bishop, N. M. Cason, E. I. Ivanov, J. M. LoSecco, A. H. Sanjari, W. D. Shephard, D. L. Stienike, S. A. Taegar, D. R. Thompson

University of Notre Dame

S. U. Chung, R. W. Hackenburg, C. Olchanski, D. P. Weygand, H. J. Willutzki

Brookhaven National Laboratory

B. B. Brabsen, R. R. Crittenden, A. R. Dzierba, J. Gunter, R. Lindenbusch, D. R. Rust, E. Scott, P. T. Smith, T. Sulanke, S. Teige

Indiana University

S. P. Denisov, V. A. Dorofeev, I. A. Kachaev, V. V. Lipaev, A. V. Popov, D. I. Ryabchikov

IHEP Protvino

Z. Bar-Yam, J. P. Dowd, P. Eugenio, M. Hayek, W. Kern, E. King

University of Massachusetts Dartmouth

V. A. Bodyagin, O. L. Kodolova, V. L. Korotkikh, M. A. Kostin, A. I. Ostrovidov, L. I. Sarycheva, N. B. Sinev, I. N. Vardanyan, A. A. Yershov

Moscow State University

D. S. Brown, T. K. Pedlar, K. K. Seth, J. Wise, D. Zhao

Northwestern University

G. S. Adams, J. P. Cummings, J. Kuhn, J. Napolitano, M. Nozar, J. A. Smith,
D. B. White, M. Witkowski

Rensselaer Polytechnic Institute

(January 21, 1998)

Abstract

A partial-wave analysis of 9082 $\eta\pi^+\pi^- n$ events produced in the reaction $\pi^- p \to \eta\pi^+\pi^- n$ at 18.3 GeV/c has been carried out using data from experiment 852 at Brookhaven National Laboratory. The data is dominated by $J^{PC} = 0^{-+}$ partial waves consistent with observation of the $\eta(1295)$ and the $\eta(1440)$. The mass and width of the $\eta(1295)$ was determined to be 1282 ± 5 MeV and 66 ± 13 MeV respectively while the $\eta(1440)$ was observed with a mass of 1404 ± 6 MeV and a width of 80 ± 21 MeV. Other partial waves of importance include the 1^{++} and the 1^{+-} waves. Results of the partial wave analysis are combined with results of other experiments to estimate $f_1(1285)$ branching fractions. These values are considerably different from current values determined without the aid of amplitude analyses.

I. INTRODUCTION

This paper presents results of a partial-wave analysis of the $\eta\pi^+\pi^-$ system in the 1.21 to 1.53 GeV/c^2 mass region. Specifically the reaction

$$\pi^- p \to \eta\pi^+\pi^- n, \quad \eta \to 2\gamma \tag{1}$$

is examined at 18.3 GeV/c. The data sample was collected during the summer of 1994 using the Multi-Particle Spectrometer (MPS) at the Alternating Gradient Synchrotron (AGS) facility of Brookhaven National Laboratory (BNL).

The identification of the isoscalar members of the $J^{PC} = 0^{-+}$ and 1^{++} nonets has been the subject of considerable interest, particularly with regard to searches for exotic mesons. It is known that some such states have $a_0(970)\pi$ decay modes. Since the $a_0(970)$ couples to both $\eta\pi$ and to $K\overline{K}$ final states, comparison of the resonances produced in the $\eta\pi^+\pi^-$ and $K\overline{K}\pi$ reactions can lead to important information with regard to this identification.

The $\eta\pi^+\pi^-$ system is complicated, characterized by the large range of accessible quantum numbers ($J^{PC} = 0^{-+}$, 0^{--}, 1^{--}, 1^{+-}, 1^{++}, 2^{--} ...), a large number of possible $\eta\pi$ and $\pi\pi$ intermediate isobars (a_0, a_2, f_0/σ, ρ, f_2), and the presence of overlapping resonances (f_1, $\eta(1295)$).

Historically, the region around the 1.3 GeV/c^{2}enhancement in the $\eta\pi^+\pi^-$ and $K\overline{K}\pi$ mass spectra was called the D region. Most early analyses of this region [1–6] made the assumption that a single state existed in the D region in the presence of an incoherent (non-interfering) background. The problem was then the determination of the appropriate quantum numbers of this state and its branching ratio to $\eta\pi^+\pi^-$. Most early experiments showed a preference for $J^{PC} = 1^{++}$ quantum numbers of the D, now referred to as the $f_1(1285)$.

Later, sufficiently high statistics were collected to carry out a partial wave analyses of the $\eta\pi^+\pi^-$ system. Stanton *et al.* [7] performed an analysis of the reaction $\pi^- p \to \eta\pi^+\pi^- n$ at 8.45 GeV/c. The D region was fit with a combination of 0^{-+}, 1^{++}, and 1^{+-} partial waves. Their analysis suggested the presence of a new state with $J^{PC} = 0^{-+}$, the $\eta(1295)$ in the D region as well as the $f_1(1285)$. In addition, it was suggested that the fit could be improved considerably if the 0^{-+} partial waves were not allowed to interfere with the other waves in the fit.

The KEK-E179 collaboration performed two partial wave analyses [20,21] of the same reaction at 8 GeV/c. They too used a set of 0^{-+}, 1^{++}, and 1^{+-} partial waves to describe the D region. Their analysis observed the $f_1(1285)$ and $\eta(1295)$ in the D region. Their analysis also suggested the presence of an additional state, the $\eta(1440)$ located in what has been called the E region.

II. APPARATUS

Figure 1 shows the experimental layout. The detector system consists of a charged-particle spectrometer and a downstream 3045-element lead-glass electromagnetic calorimeter (LGD) [8] [9] to provide neutral particle detection.

An 18.3 GeV/c π^- beam is incident on the 30-cm liquid-hydrogen target located at the center of the MPS magnet. Surrounding the target is a 198-element thallium-doped cesium iodide cylindrical veto array (CsI) [10] used in off-line analysis to reject events with wide-angle, low-energy photons from baryonic resonance decay. Between the target and the CsI is a four-plane cylindrical drift chamber (TCYL) [11] for triggering on recoil charged tracks. The downstream half of the magnet is equipped with three proportional wire chambers (TPX1-3) for triggering on forward charged-track multiplicity, and six drift chamber modules (DX1-6) for measuring the momentum of forward charged tracks. Also in the magnet is a window-frame lead-scintillator sandwich photon veto counter (DEA) which covers the solid-angle gap between the CsI and the LGD. Two scintillation counters are mounted on DEA, a window-frame counter (CPVC) to distinguish between charged and neutral particles hitting DEA, and a rectangular counter (CPVB) which covers the hole in the DEA and is used, in conjunction with CPVC, to veto charged tracks in the all-neutral trigger. Beyond the magnet and just upstream of the LGD is a final drift chamber (TDX4) consisting of two X-planes, and two scintillation counters (BV and EV) for vetoing non-interacting beam particles and elastic-scatter events. Further details regarding the equipment are given elsewhere [12].

III. DATA SELECTION AND PROPERTIES

The trigger for the $\eta\pi^+\pi^-$ topology required a Ĉerenkov-tagged π^- incident on the target, two charged tracks emerging from the target, no charged recoil track, and an effective mass greater than that of the π^0 in the LGD as determined by a hardware processor. Some 48 million triggers of this type were taken. From these, a final sample of 9082 events consistent with reaction 1 were selected by requiring:

- less than 20 MeV in the CsI to enhance recoil neutron events over N^* events;
- exactly two photons (η) reconstructed in the LGD;
- a reconstructed beam track;
- two forward charged tracks of opposite charge;
- no recoil charged track;
- a 3-constraint SQUAW [13] kinematic fit to reaction 1 with a confidence level greater than 7%;
- $|t| < 3$ GeV^2/c^2 after kinematic fitting.

The two-gamma mass distribution for about 10% of the data is shown before and after the data selection cuts in Fig. 2. [1] The η signal is nearly background free after cuts.

The corrected mass distribution for these events is shown in Figure 3. Evident is the η' which, when fit to a Gaussian, yields a mass of 961 MeV with σ =10 MeV, indicative

[1] A cut was made on the missing-mass-squared distribution in Fig. 2b to simulate the effect of the SQUAW kinematic fitting.

of the resolution of the apparatus in the 1 GeV/c^2 mass region. An enhancement in the D region[2] is observed which, when fit to a Gaussian plus a linear background, yields a mass of 1278 MeV and $\sigma = 20$ MeV.

Shown in Figs. 4a and 4b respectively are the $\eta\pi^-$ and $\eta\pi^+$ effective mass distributions respectively for a three-body mass between 1.2 and 1.54 GeV/c^2. Seen in each spectrum are $a_0(980)$ peaks. If we restrict ourselves to the D region (1.2-1.35 GeV/c^2), show in figure 5, we can see that the two body mass distributions vary as a function of $\eta\pi\pi$ mass. Specifically an asymmetry is observed between the of a_0^+ and a_0^-. This asymmetry is due to due to the interference between odd and even isospin states and is well-described in the partial-wave analysis described in the next section.

The $\pi^+\pi^-$ effective mass distribution for the 1.1-2.0 GeV/c^2 three-body mass region is shown in Fig. 4c. Evident is a distorted $\rho(770)$ signal due to its proximity to threshold.

For the following analysis, 9,082 events were selected from the above data set in the low-mass region. These events have $1.205 \leq M(\eta\pi\pi) \leq 1.535$GeV/c^2.

IV. PARTIAL-WAVE ANALYSIS

A. Fitting Procedure

The formalism used in this analysis is based on the papers of Chung [14] and Chung and Trueman [15]. The analysis techique involved the use of the reflectivity basis to describe the individual partial waves and the maximization of an extended log likelihood function in the fitting proceduere. The procedure and analysis programs are described by Cummings and Weygand [16].

Due to the large number of possible partial waves accessible to the $\eta\pi^+\pi^-$ system, a complete analysis requiring all possible isobars and partial waves is not practical given the

[2] A detailed description of the Dalitz plot in the D region is given is elsewhere [12].

limited statistics. In principal one would like to include all possible isobars: a_0, a_2, f_0, ρ, f_2 and a large set of partial waves ($J < 4$). Because this analysis is in the low-mass region, we can eliminate the a_2 and the f_2 isobars. Furthermore, we choose to consider only amplitudes with $J < 2$ since there are no known states[3] with higher spin in this low-mass region which decay to $\eta\pi\pi$.

An incoherent background was included in some fits. This was represented by a single real parameter with no angular dependence associated with it (other than the acceptance of the apparatus). While the final fit did not contain a background term, its use was explored in the fitting process. The background is in many ways similar to a non-interfering $J = 0$, $\sigma\eta$ partial wave, making them quite difficult to differentiate.

In principal, a rank 2 fit is required to describe the data to account for the presence of spin-flip and non-flip amplitudes generated at the baryon vertex. Fits were attempted for both rank 1 and 2. The likelihood function was improved greatly when the fit rank was increased to two. In addition, rank 1 fits to the data became unstable in the absence of a background wave. Furthermore, when a background was included, it had unexpected structure in the D and E regions and occurred at a higher level than anticipated. All of this information suggested that a rank 2 fit was required to fit the data, and rank 1 fits were not used.

The ρ isobar was modeled by a relativistic Breit-Wigner with parameters extracted from the Particle Data Book [17]. For the final fit the a_0 was modeled as a Breit-Wigner form with a mass of 980 MeV and a width of 72 MeV. The $\pi\pi$ S-wave (the σ/f_0) was represented by a parameterization of the $\pi^+\pi^-$ S-wave provided by K. L. Au *et al.* [18]. Alternate parameterizations of the a_0 and the σ/f_0 were explored [19]. However it was found that the particular choice of parameterization had little effect on the final result.

---

[3]The $f_2(1270)$ could in principle reach this final state through the $a_2\pi$ mode, but this is highly suppressed by phase space.

To determine the appropriate waves over the low-mass region, a fit was performed using a coarse bin width of 50 MeV with all waves with $J < 2$ included. Waves were then discarded from the fit if their removal had little effect on the value of the likelihood function ($|\Delta\mathcal{L}| < 5$). Selected waves were then re-introduced in the fit to insure the stability of the solution. In total, several hundred different sets of partial waves were fit. For each combination of partial waves, the binning, t cuts, starting values, and starting point were varied to insure stability of the final solution. The set of waves chosen for the final fit is shown in Table I.

For the final fit, a bin width of 30 MeV was chosen. This was seen as a compromise between achieving adequate statistics in each mass bin and acquiring the best possible resolution in the D and E regions. The starting values of the fit were randomly chosen and the entire spectrum was re-fit several times to insure stability with the finer bin width. For bin widths below 30 MeV the fits often became unstable, converging to different solutions depending upon the starting values.

It is interesting to note that the final waves selected for the low mass-region are consistent with those used by Stanton *et al.* [7] and by Fukui *et al.* [20]. The only exception is that we do not use a 1^{+-} $a_0\pi$ wave. We found that the fit could not distinguish this wave from the 1^{+-} $\rho\eta$ wave in the D region. Due to the unambiguous presence of the $\rho\eta$ partial wave at higher mass, it was decided not to include the 1^{+-} $a_0\pi$ partial wave in the final set.

B. Results of Partial Wave Analysis

1. $J^{PC} = 0^{-+}$ *Partial Waves*

The fitted intensity distribution for the 0^{-+} $a_0\pi$ wave as a function of $\eta\pi^+\pi^-$ effective mass is shown in Fig. 6a. A sharp peak in the D region is evident, consistent with the observation of $\eta(1295) \to a_0\pi$. Some intensity is seen extending out to 1.4 GeV/c^2. It should be noted that the majority of the signal for this wave comes from the second rank of the fit. This indicates a different production mechanism than that for the 1^{+-} and the 1^{++}

waves (which are produced dominantly in the first rank) and means that these latter waves do not interfere with the 0^{-+} wave.

Shown in Fig. 6b, the $0^{-+}\sigma\eta$ wave is double-peaked, with enhancements in both the D and E regions. This structure is suggestive of $\eta(1295)$ and $\eta(1440)$ production. In fact, the majority of the structure seen in the E region is associated with this wave. This result, is somewhat inconsistent with previous analyses [20,21], which observe the presence of a $\sigma\eta$ decay of the $\eta(1440)$, but do not see it dominating the structure in the E region.

As was mentioned above, second-rank fits were required to obtain good fits to the data. A large portion of the 0^{-+} signal occurred in the second rank, with the largest proportion in the $0^{-+}\sigma\eta$ partial wave in the E region. Because these waves do not interfere with the other dominant waves in the fit, reliable relative phase motion could not be obtained.

The result of adding the two 0^{-+} waves coherently in each rank and then adding the sums incoherently is shown in Fig. 6c. Peaks in the D and E regions are clearly visible, and constructive interference occurs within each rank. The spectrum was fit to two spin-0 Breit-Wigners plus a quadratic background. Fitted values of the masses and widths are given in Table II. In addition, the $a_0\pi/\sigma\eta$ branching ratio can be determined from Fig. 6 for both the $\eta(1295)$ and the $\eta(1440)$. These values are also given in Table II.

2. $J^{PC} = 1^{++}$ Partial Waves

Shown in Fig. 7a is the 1^{++} $a_0\pi$ partial wave intensity distribution. This wave shows evidence for the f_1. However, the amount of f_1 signal is surprisingly small (600 counts in the peak bin) compared with the 0^{-+} intensity. No significant structure was observed at higher mass.

Figure 7b shows the 1^{++} $\sigma\eta$ partial wave intensity distribution. This wave was necessary to the fit for bins above 1.45 GeV/c^2.

Shown in Fig. 7c is the coherent sum of the 1^{++} partial waves. This sum displays a peak in the vicinity of the f_1 and a slow rise at high mass. When a comparison to the coherent sum of the 0^{-+} partial waves (Fig. 6) is made one observes that the majority of signal in the D and E regions arises not from 1^{++} partial waves but from the 0^{-+} wave. This observation is especially important to the D region, because some previous analyses used for branching ratio estimates have assumed the D signal to be primarily 1^{++}, not 0^{-+}.

3. $\rho\eta$ Partial Waves

The intensity distribution for the $1^{+-}\rho\eta$ wave is shown in Fig. 8a. This wave was seen in all previous analyses and is significant over the low mass region. Previous experiments [20] have claimed this wave to be evidence for production of the $b_1(1235)$ with a $\rho\eta$ decay mode. However the lack of structure in the 1^{+-} wave and unclear phase motion discourage this interpretation. It should be noted that this wave is essential for producing the a_0^+/a_0^- asymmetry observed in the data.

Shown in Fig. 8b is the $1^{--}\rho\eta$ intensity distribution. This is the only negative reflectivity partial wave and does not interfere with any other partial waves in the fit. The wave steadily increases throughout the low-mass region and its behavior is consistent with it being the low-mass tail of the $\rho(1700)$.

V. DISCUSSION OF THE $F_1(1285)$ BRANCHING FRACTIONS

The $\eta(1295)$ production dominates the D peak, accounting for roughly 80% of the D signal. This observation has implications on the $f_1 \to \eta\pi\pi$ branching fraction. Previous experiments [2] have determined the $f_1 \to \eta\pi\pi$ branching fraction without the aid of a partial wave analysis under the assumption that the D peak consists of a single f_1 state, resting on top of an incoherent background. This assumption is clearly incorrect, and values for the branching fractions must be corrected.

Corden *et al.* [2] studied the reactions $\pi^- p \to \eta\pi^+\pi^- n$ and $\pi^- p \to K\overline{K}\pi n$ at 15 GeV/c. In their analysis they obtained a $K\overline{K}\pi/\eta\pi\pi$ branching ratio in the D region of 0.5 ± 0.2 without the aid of a partial wave analysis. It is reasonable to assume that the relative production of f_1 and $\eta(1295)$ is the same in this experiment as in that of Ref. [2] since the experiments are close in energy and are studying the same final state. It is also reasonable to assume that the $K\overline{K}\pi$ decay mode is all due to f_1 decay since this reaction has been studied using a partial wave analysis [22] with this conclusion. Thus the $K\overline{K}\pi/\eta\pi\pi$ branching ratio of the f_1 should be adjusted by dividing the observed D-region $K\overline{K}\pi/\eta\pi\pi$ branching ratio by the fraction of the D peak which is due to $f_1(1285)$ decay. We thus obtain $(0.5 \pm 0.2)/0.2 = 2.5 \pm 1.0$ for this branching ratio.

We can perform the same type of estimate using, instead of our own analysis, the results of KEK-E179 [20] for the reaction $\pi^- p \to \eta\pi^+\pi^- n$ at 8.95 GeV/c. In that experiment, the fraction of the D peak which is due to $f_1(1285)$ decay is 50%. Again using the results of Corden *et al.* (although in this case the difference in the energies of the experiments is larger) one can obtain an alternate estimate of the $K\overline{K}\pi/\eta\pi\pi$ branching ratio for f_1 decay to be 1.0 ± 0.4.

One can estimate the effect which these results can have on the $f_1(1285)$ branching fractions by assuming that the D signal observed in the $K\overline{K}\pi$, $\gamma\rho^0$, and 4π decay modes is due only to f_1 decay. This is the most reasonable for the $K\overline{K}\pi$ mode as mentioned above. However, the other two decay modes ($\gamma\rho^0$, 4π) have not been as thoroughly investigated [4]. Specifically, using the quoted branching ratios of 0.33 ± 0.04 for $K\overline{K}\pi/4\pi$ and 0.45 ± 0.18 for $\gamma\rho^0/2\pi^+2\pi^-$, the $f_1(1285)$ branching fractions can be calculated. In Table III are listed the f_1 branching fractions calculated using $K\overline{K}\pi/\eta\pi\pi$ branching ratios of 2.5 ± 1.0 (BNL-E852) and 1 ± 0.4 (KEK-E179) respectively.

Assigning systematic errors to these $f_1(1285)$ branching fractions is difficult due to the undetermined uncertainties in branching ratios for the 4π and $\gamma\rho^0$ decay modes. However it is clear from this exercise that the $f_1(1285)$ branching fractions as listed in the particle

---

[4]Of these modes the 4π branching fraction is most suspect due to the large number of interfering partial waves which contribute to a 4π data set.

data book need to be corrected. The 4π decay mode is probably the dominant decay mode of the f_1 rather than the $\eta\pi\pi$ mode.

VI. SUMMARY AND CONCLUSIONS

The low-mass partial wave analysis was performed on 9082 events in the 1.20–1.54 GeV/c^2 mass interval. This analysis used a rank 2 fit with 30 MeV bins and a set of 6 partial waves. The partial waves used in the fit were: $0^{-+}a_0\pi$, $0^{-+}\sigma\eta$, $1^{+-}\rho\eta$, $1^{++}a_0\pi$, $1^{++}\sigma\eta$ and $1^{--}\rho\eta$.

The D region was found to include a large contribution from the 0^{-+} wave peaking at a mass consistent with the presence of the $\eta(1295)$. Some evidence of 1^{++} wave was also seen, consistent with $f_1(1285)$ production. The fact that the region is dominated by $\eta(1295)$ production leads to significant changes in the $f_1(1285)$ branching fractions discussed in Section V.

The $\eta(1295)$ was seen to decay to both $a_0\pi$ and $\sigma\eta$. The $a_0\pi/\sigma\eta$ branching ratio for $\eta(1295)$ was estimated to be 0.48 ± 0.22. The mass and width of the $\eta(1295)$ were determined to be 1282 ± 5 MeV and 66 ± 13 MeV respectively. This result is consistent with that of Fukui *et al.* [20] who determined the mass and width of the $\eta(1295)$ to be 1295 ± 4 MeV and 53 ± 6 MeV.

The E region is dominated by a large $0^{-+}f_0/\sigma\eta$ signal present in the second rank of the fit. This signal is consistent with production of a single state, the $\eta(1440)$. The mass and width of the $\eta(1440)$ are estimated to be 1404 ± 6 MeV and 80 ± 21 MeV. This result is remarkably consistent with the Particle Data Group weighted average value for the mass and width of the $\eta(1440)$ of 1415 ± 10 MeV and 60 ± 20 MeV.

Previous analysis of the reactions $\pi^- p \to K\overline{K}\pi n$ and in J/ψ decays have observed 0^{-+} structures in the E region in the $a_0\pi$ and K^*K decay modes while studies of the $\pi^- p \to \eta\pi^+\pi^- n$ reaction have yielded both a $\sigma\eta$ and an $a_0\pi$ component of the E as in this analysis. However, the $\sigma\eta$ signal in this analysis dominates the E region, while previous analyses (KEK-E179) have suggested a larger $a_0\pi$ component of the E. An estimate of the $\eta(1440)$ $a_0\pi/\sigma\eta$ branching ratio from this analysis is 0.15 ± 0.04. The systematic errors are unassigned but assumed to be large due to the difficulty of the fit in distinguishing $0^{-+}a_0\pi$ and $0^{-+}\sigma\eta$ waves from each other.

In addition to the $f_1(1285)$, $\eta(1295)$ and the $\eta(1440)$ contributions, a large, relatively structureless signal in the $1^{+-}\rho\eta$ wave was observed throughout the low mass region. This wave has also been observed in all previous partial wave analyses of the $\pi^-p \rightarrow \eta\pi^+\pi^-n$ system. There is no obvious resonance interpretation of this structure, but its presence is required to account for the large a_0^+/a_0^- production asymmetry seen in the D region, indicative of odd-even isospin interference. A $1^{--}\rho\eta$ partial wave is also seen in the low-mass fit, consistent with the low-mass tail of the $\rho(1700)$.

We would like to express our deep appreciation to the members of the MPS group. Without their outstanding efforts, the results presented here could not have been obtained. We would also like to acknowledge the invaluable assistance of the staffs of the AGS and BNL, and of the various collaborating institutions. This research was supported in part by the National Science Foundation and the US Department of Energy.

REFERENCES

[1] J. H. Campbell *et al*, Phys. Rev. Lett. **22**, 1204 (1969)

[2] M. J. Corden *et al.*, Nucl. Phys. B **144**, 153 (1978)

[3] O. I. Dahl *et. al*, PR, 1967, vol. 164, pp1377–1429

[4] R. Nacasch *et. al*, Nucl. Phys. B **203**, 203 (1978)

[5] C. Defoix *et. al*, Nucl. Phys. B **44**, 125 (1972)

[6] A. Gurtu *et al.*, Nucl. Phys. B **151**, 181 (1979)

[7] N. R. Stanton *et al.*, Phys. Rev. Lett.**42**, 346 (1979)

[8] B. Brabson *et al.*, Nucl. Instr. & Meth A **332**, 419 (1993)

[9] R. R. Crittendon, Nucl. Instr. & Meth A, **387**, 377 (1997)

[10] T. Adams *et al.*, Nucl. Instr. & Meth A **386**, 617 (1996)

[11] Z. Bar-Yam *et al.*, Nucl. Instr. & Meth A **342**, 398 (1994)

[12] S. Teige *et al.*, to be published 1998

[13] O. I. Dahl *et al.*, "SQUAW kinematic fitting program", Univ. of California, Berkeley Group A programming note P-126, unpublished (1968).

[14] S.U. Chung, "Formulas for Partial-Wave Analysis", Brookhaven BNL-QGS-93-05, unpublished (1993).

[15] S.U. Chung and T.L. Trueman, Phys. Rev. D **111**, 633 (1975)

[16] J. P. Cummings and D. P. Weygand, "The New BNL Partial Wave Analysis Programs", BNL-64637, unpublished (1997).

[17] Particle Data Group, Phys. Rev. D **50**, (1996)

[18] K. L. Au *et al.*, Phys. Rev. D **35**, 1633 (1986)

[19] C. Amsler *et al.*, Phys. Lett. B **335**, 425 (1995)

[20] S. Fukui *et al.*, Phys. Rev. B **267**, 293 (1991)

[21] A. Ando *et al.*, Phys. Rev. Lett. **57**, 1296 (1986)

[22] A. Birman *et al.*, Phys. Rev. Lett. **61**, 1557 (1988)

FIGURES

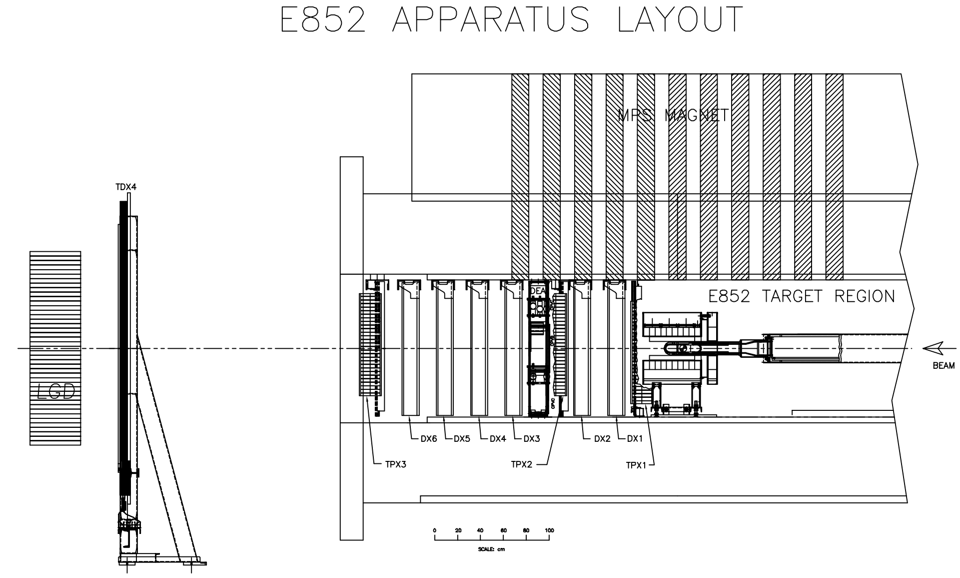

FIG. 1. E852 Apparatus Layout

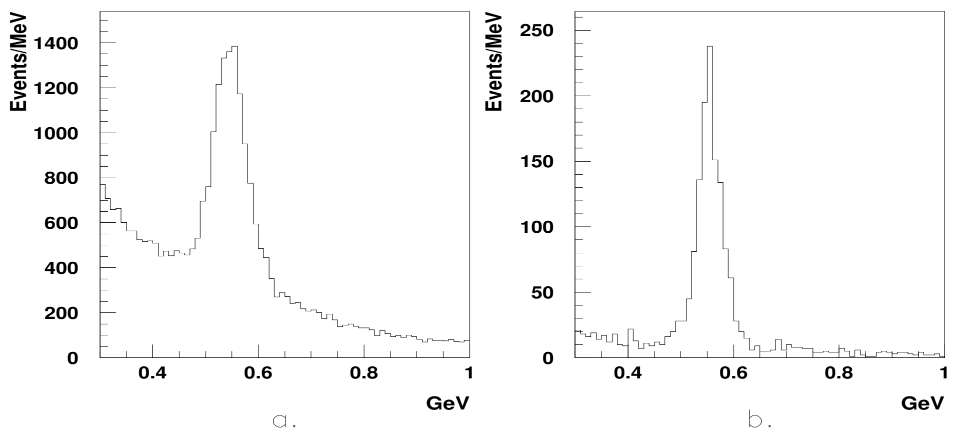

FIG. 2. a: 2γ mass distribution before cuts, b: 2γ mass after data selection cuts

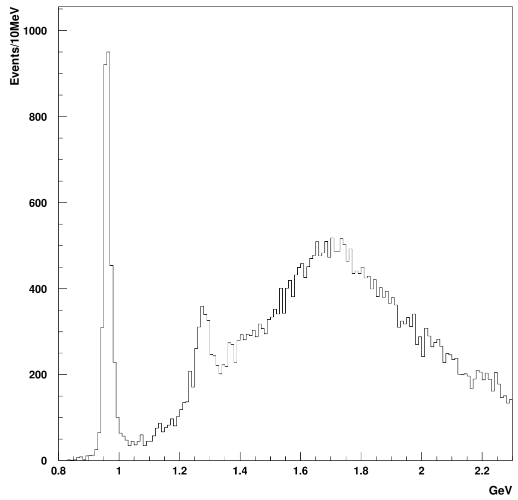

FIG. 3. $\eta\pi^+\pi^-$ three body mass distribution

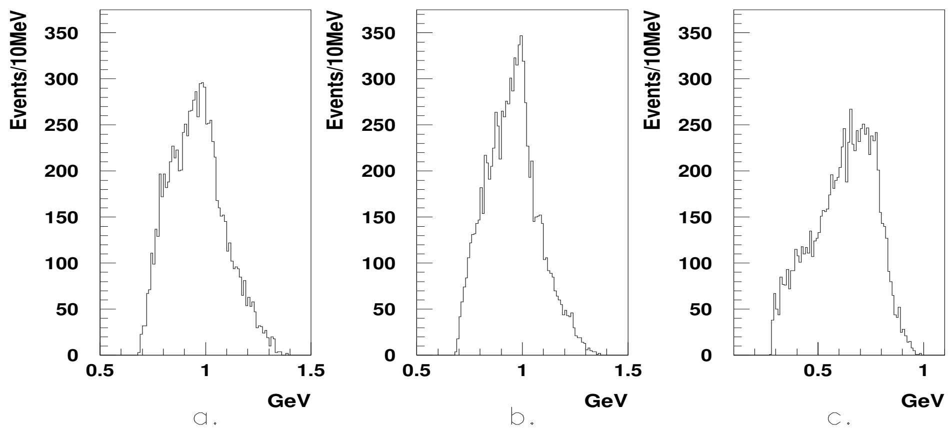

FIG. 4. a: $\eta\pi^-$ two-body mass distribution, b: $\eta\pi^+$ two-body mass distribution, c: $\pi^+\pi^-$ two-body mass distribution for the $\eta\pi^+\pi^-$ massregion between 1.2 and 1.54 GeV/c^2.

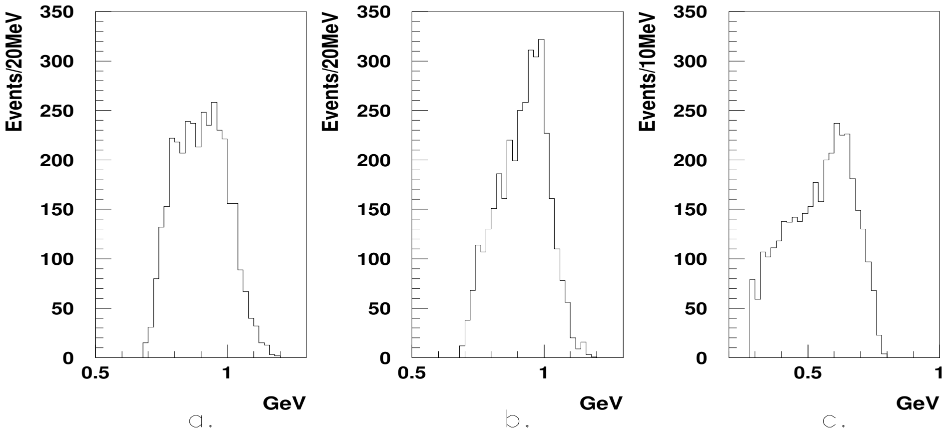

FIG. 5. a: $\eta\pi^-$ two-body mass distribution (D region), b: $\eta\pi^+$ two-body mass distribution (D region), c: $\pi^+\pi^-$ two-body mass distribution for the $\eta\pi^+\pi^-$ mass region between 1.2 and 1.35 GeV/c^2 (D region).

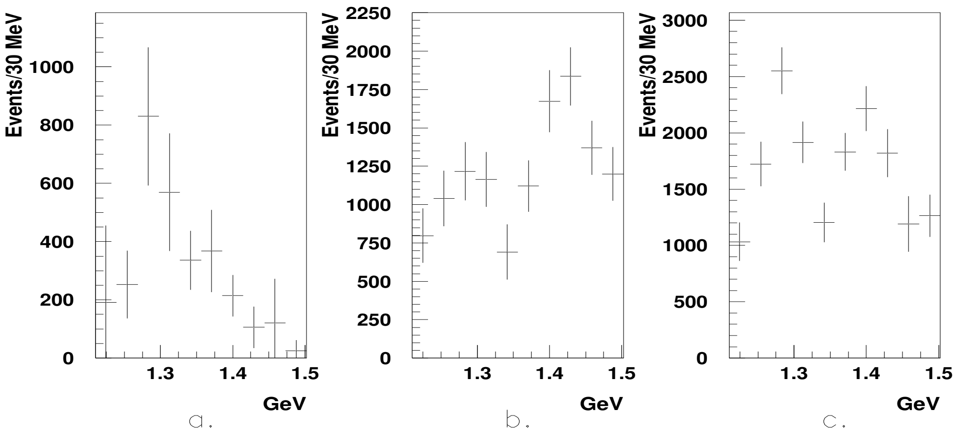

FIG. 6. a: $0^{-+}a_0\pi$ intensity, b: $0^{-+}\sigma\eta$ intensity, c: Total 0^{-+} intensity

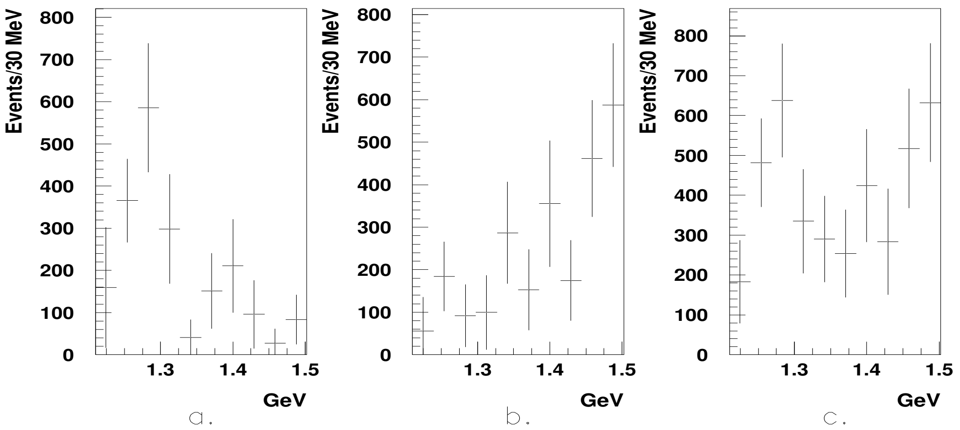

FIG. 7. a: $1^{++}a_0\pi$ intensity, b: $1^{++}\sigma\eta$ intensity, c: Total 1^{++} intensity

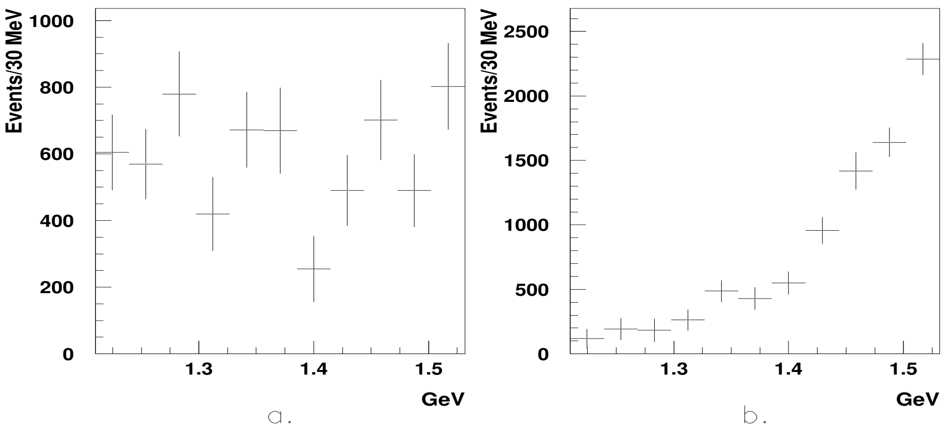

FIG. 8. a: $1^{+-}\rho\eta$ intensity, b: $1^{--}\rho\eta$ intensity (negative reflectivity partial wave)

TABLES

TABLE I. Partial Waves Used in Final Fit

$Isospin$	J^{PC}	Isobar	l	m	ϵ
1	1^{--}	ρ	1	0	-1
0	0^{-+}	a_0	0	0	$+1$
0	0^{-+}	σ	0	0	$+1$
0	1^{++}	a_0	1	0	$+1$
0	1^{++}	σ	1	0	$+1$
1	1^{+-}	ρ	0	0	$+1$

TABLE II. Properties of the $J^{PC} = 0^{-+}$ States

	Mass (GeV/c^2)	Width (GeV/c^2)	$a_0\pi/\sigma\eta$ Branching Ratio
$\eta(1295)$	1.282 ± 0.005	0.066 ± 0.013	0.48 ± 0.22
$\eta(1440)$	1.404 ± 0.006	0.080 ± 0.021	0.15 ± 0.04

TABLE III. f_1 Branching Fractions

Decay Mode	PDG	BNL-E852	KEK-E179
4π	$29 \pm 6\%$	$59 \pm 17 \pm ?\%$	$53 \pm 21 \pm ?\%$
$\eta\pi\pi$	$54 \pm 15\%$	$8 \pm 3 \pm ?\%$	$17.5 \pm 9 \pm ?\%$
$\gamma\rho^0$	$6.6 \pm 1.3\%$	$13 \pm 8 \pm ?\%$	$12 \pm 7 \pm ?$ %
$K\overline{K}\pi$	$9.7 \pm 1.6\%$	$20 \pm 7 \pm ?\%$	$17.5 \pm 7 \pm ?\%$